Optics & Laser Technology 158 (2023) 108875

Contents lists available at ScienceDirect

Optics and Laser Technology

journal homepage: www.elsevier.com/locate/optlastec

Full length article

Investigating the mechanical properties and fusion zone microstructure of dissimilar laser weld joint of duplex 2205 stainless steel and A516 carbon steel

Alireza Karimi [a,b], Arash Karimipour [a,b,*], Mohammad Akbari [a,b], Mohammad Mehdi Razzaghi [b,c], Mehdi Jamali Ghahderijani [a,b]

[a] Department of Mechanical Engineering, Najafabad Branch, Islamic Azad University, Najafabad, Iran
[b] Aerospace and Energy Conversion Research Center, Najafabad Branch, Islamic Azad University, Najafabad, Iran
[c] Department of Aerospace Engineering, Najafabad Branch, Islamic Azad University, Najafabad, Iran

ARTICLE INFO

Keywords:
Dissimilar laser welding
Duplex stainless steel
Fusion zone microstructure
Tensile strength

ABSTRACT

Laser welding of dissimilar A516 low carbon steel and duplex stainless steel was conducted to evaluate the effect of fiber laser welding parameters (e.g., laser power, welding speed, nozzle distance and beam deviation) on the responses of tensile strength, depth of the melt pool, microstructure, temperature near the melt pool and melt pool hardness. The maximum tensile strength of 500 MPa and 18 percent elongation were obtained at the laser power of 400 W, welding speed of 300 mm/min and the focal point. The absorbed power of laser and linear speed of welding had the most notable impact on the tensile strength of the weld. The fusion zone microstructure was composed of a combination of ferrite–austenite distribution from duplex stainless steel (DSS) based on different cooling and heating cycles. During the nucleation process, ferrite grains were transformed to austenite grains from different areas of the fusion zone. Also, the weld fusion zone microstructure at A516 side was composed of fully martensitic structure, according to the higher heat input upper critical temperature of steel (AC3), thereby leading to rapid cooling. The EDS analysis also showed that the Fe percentage was continually reduced at the fusion line from A516 to DSS, although Ni and Cr were distributed at the fusion zone with some minor changes of weight percentage. Therefore, Cr and Ni had a crucial effect on elemental alloy composition in this laser welding process. The ductility of the A516 fracture surface with bigger and deeper fracture dimples was caused by applying higher laser energy density, which effectively improved the fracture ductility of the welded samples.

1. Introduction

Duplex Stainless Steels (DSS) have vast applications in such varied areas as gas, oil and petrochemical, marine and vehicle production industries because of providing superior corrosion resistance and the same balance of austenite and ferrite distribution in the microstructure [1,2]. Thus, the demand for welding DSS has been rising significantly to meet the industrial requirements to improve both metallurgical properties and productivity of these joints. Conventional welding of super duplex stainless steels (SDSS) may alter the distribution of the ferrite–austenite microstructure, which could have impact on the resultant weld fusion zone properties [3]. Duplex stainless steel 2205 has been considered for its many industrial applications due to its unique properties, in comparison to the conventional austenitic and ferritic stainless steels [4]. Saravanan et al. [5] studied the interaction effect of both laser power and welding speed on the resultant temperature and hence, the weld zone microstructure and mechanical properties of the super duplex steel welded by a pulsed YAG laser. Full penetration was observed at higher heat input rates.

Adomako et al. [6] also studied the quality of dissimilar CoCrFeMnNi-HEA and duplex stainless steel laser welded joints. CoCrFeMnNi-HEA showed a heat-affected zone with CrMn oxide inclusions. They proposed a technique for offset welding to enhance the dissimilar joint strength. Ahmad et al. [7] also studied Inconel 625 and DSS 2205 supperalloys at different levels of heat inputs. The weld joint microstructure was comprehensively analyzed. The weld joint was composed of Cellular dendritic and columnar dendritic grains. Defects such as solidification cracks or porosity were not observed in the weld

* Corresponding author at: Department of Mechanical Engineering, Najafabad Branch, Islamic Azad University, Najafabad, Iran.
E-mail address: arashkarimipour@gmail.com (A. Karimipour).

https://doi.org/10.1016/j.optlastec.2022.108875
Received 7 September 2022; Received in revised form 29 October 2022; Accepted 1 November 2022
Available online 9 November 2022
0030-3992/

Table 1
Mechanical properties of welded samples [30].

material	A516 steel	Duplex 2205
Physical Properties		
Ultimate Tensile Strength	485–620 MPa	621 MPa
Yield Tensile Strength,	260 MPa	445 MPa
Elongation (%)	17	17

metal microstructure.

Further, Baghdadchi et al. [8] studied the laser reheating impact on the welding of FDX 27 duplex stainless steel. Pure nitrogen was applied as a shielding gas to improve the formation of austenite and reduce the possibility of nitride formation in DSS welds. Calliari et al. [9] also focused on pulsed laser welding of plastically deformed 2304 to investigate the peak power effect on the microstructure and penetration rate of the joint. Further, Chen et al. [10] studied the effects of different combinations of power and speed at an identical line energy on dissimilar metals 316 L/GH909 laser welding. Different melt pool dimensions were verified by the simulation of the temperature field. Ghorsh et al. [11] also experimentally studied Nd: YAG laser butt welding of 2205 Duplex steel. They concluded that the increase in pulse width decreased the weld strength and bead width. Gozarganji et al [12] also studied the effect of nitrogen shielding gas mixture on pulsed laser weld microstructure and hardness of 2205 duplex stainless steel. Light and scanning electron microscopy were then used to study the resulting microstructures. They found that the hardness values were increased from 280 HV in the base metal to 307 HV in the weld center line; however, the weld hardness was not significantly influenced by the shielding gas mixture. In addition, Landowski [13] studied the effects of welding parameters on the microstructure, weld geometry and bead shape of the welded stainless steel. A clear correlation was proposed between the weld penetration depth and focal point position.

Furthermore, Sivagurumanikandan et al. [14] analyzed the effect of the welding linear speed, laser beam average incident power and position of the focal point on the weld strength of SDSS through response surface methodology and neural network. They reported that the optimum condition was attained at the power of 550 W, laser frequency of 13 Hz, welding speed of 136 mm/min and the focal position of 0 mm to reach a higher tensile strength.

Oyyaravelu et al. [15] also investigated the microstructure and mechanical properties of.

Nd:YAG laser welded high strength low alloy (HSLA) SA516 grade 70 boiler steel. The martensite phase in the weld fusion zone was observed in the fusion zone due to the faster cooling rate of the laser weldment. They proposed a correlation between the microstructure of the weld joints and their mechanical properties. Salavati et al. [16] also investigated the effects of the parameters variations on the mechanical properties and microstructural changes of the weld joint. They reported that by using nitrogen gas, a remarkable increase in micro hardness was observed.

Review of aforementioned articles and other related Refs. [17–29] showed that investigation of microstructure, mechanical properties and phase change processes has many applications in the industries. Stainless steel is generally known as one of the primarily considered materials for dissimilar laser welding. In this paper, for the first time, dissimilar laser welding of duplex stainless steel 2205 and A516 low carbon steel was investigated through the design of experiments to systematically analyze the influence of parameters on the weld metallurgical and mechanical properties. Combination of these materials at the fusion zone with different participation from different microstructural and thermophysical aspects could remarkably influence the weld joint properties; this had not been comprehensively studied before.

2. Experimental procedure

Laser dissimilar butt joint welding of duplex stainless steel 2205 and A516 steel plates (50 × 25 × 2 mm) was performed. The mechanical specifications and chemical characterization of both materials are presented in Tables 1 and 2, respectively.

A fiber laser with the maximum output power of 1 KW, which was equipped with raytools BW240 laser welding head, was utilized for the experiments. The side blow nozzle was used to apply argon gas for protecting melt pool region. The laser beam was irradiated to the alloys perpendicularly. A three axis CNC table was then used for moving and positioning the laser beam at determined locations and speeds. All samples for metallography were prepared under ASTM E3. The optical microscope, BX53M model, was used for metallography analysis. The microstructural changes from the base metals to the fusion zone were analyzed using a TESCAN-LMU scan electron microscope. The microhardness tests were then performed using ZWICK micro-hardness tester by applying the load of 100 g at 10 s time.

Tensile tests of welded and base metals were conducted using AI-7000 testing machine and the samples were prepared under ASTM E8 standard. A schematic and real view from the welding experiments while measuring temperature can be seen in Fig. 1.

3. Experimental design

The experiments were designed using the central composite design (CCD) method. Four parameters of laser power, laser welding nozzle distance from the surface of the workpiece, welding speed and deviation from the beam incident point on the workpiece surface were considered as the input variables. According to a set of primarily number of experiments (8 tests) the lower and upper limits of the process parameters were discretizing to approximately evaluate the number of the experiments and their levels. Table 3 illustrates the experimental conditions for dissimilar laser welding. Based on the primarily experiments the experimental design including number of factors and their levels were selected. These tests implied that the beam deviation could play an important role on dissimilar laser welding. In total, 28 experiments including 4 points in the center, 8 axial points and 16 cubic points were considered, as shown in Table 4. According to the selection of four distinct parameters, a total number of 27 degrees of freedom, including 10 for linear and non-linear terms, 20 for error and 17 were dedicated to the Lack of fit. The higher degree of freedom indicated that the model's error and accuracy of the nonlinear regression model were higher for estimating the test results. The CCD experimental design was also selected to investigate the influence of different process parameters on the resultant temperature near the melt pool and the tensile strength of the dissimilar joint.

Table 2
Chemical composition of the alloys [31].

	Element (% W)								
	C	Si	Mn	P	AL	Cr	Ni	Mo	s
A516	0.20	0.6	1.7	0.03	0.02	0.3	0.3	0.08	0.03
Duplex 2205 steel	0.03	1.00	2.00	0.03	–	23.0	6.5	3.5	0.02

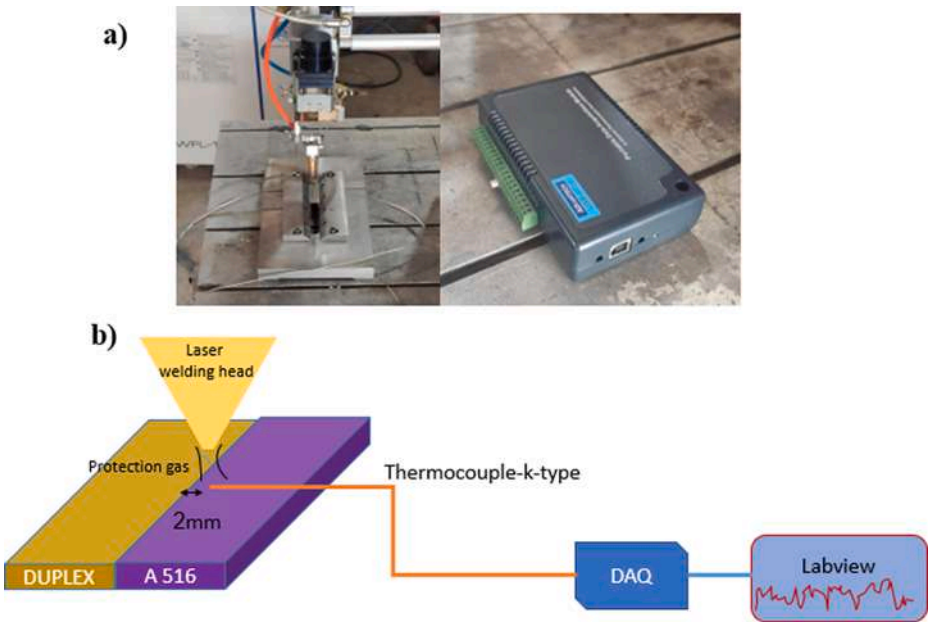

Fig. 1. Experimental configuration, (a) schematic, (b) actual view.

Table 3
Primarily experimental matrix.

Exp. No	Power (W)	Speed (mm/min)	Nozzle distance (mm)	Deviation (mm)
1	400	300	55.0	−0.5
2	300	400	50.0	−1.5
3	150	300	55.0	0.5
4	400	200	55.0	−0.5
5	250	300	50.0	−0.5
6	250	200	50.0	0.5
7	550	250	52.5	0.0

4. Result and discussion

$$Tds = 88 + 0.3606 \times Power - 0.1808 \times Speed + 0.98 \times Noz - dis - 1139 \times Dev + 0.588 \times Power \times Dev + 0.697 \times Speed \times Dev + 15.65 noz - dis \times Ddev \quad (1)$$

In order to systematically analyze the effect of the selected laser dissimilar welding process parameters on the created temperature gradient, the temperature around the melt pool at two distinct points on each metal was measured. Changes in temperature field not only could provide information on the temperate gradient on the solid part of both meals, but also indirectly indicate the dimensions of the melt pool and the clear discrepancy of the heat transfer rate of both metals. Hence, the created melt pool and the resultant joint, according to the measured temperature field of each of the metals, could be predicted.

4.1. Effect of welding parameters on the temperature field of duplex stainless steel

The major effect of laser welding parameters and their interaction, including laser power, linear welding speed, distance of nozzle and deflection of the beam, on the temperature of duplex stainless steel was analyzed. The Rsq value of 82 % and Lack of Fit 68 % indicated that the regression model was in a good agreement with the experimental data. The analysis of variance (ANOVA) results, as depicted in Table 5, also implied that incident beam power and beam deflection had a notable effect on the measured temperature at the distance of 2 mm from the molten pool center. Among the other parameters, the interaction of laser power and beam deflection had a more pronounced impact on the temperature around the molten pool of duplex stainless steel.

The temperature regression equation (Eq. (1)) near the melt pool area for duplex stainless steel includes the linear terms of laser power, speed, the distance of nozzle and power interaction, and the distance with the beam deflection from the contact point of the two parts. Some square terms of power, speed and distance of nozzle were eliminated due to being insignificant in analysis of variance. These terms had more than three decimal digits which in turn seems to be eliminated to reach a simpler form of the equation.

Fig. 2 clearly illustrates the effect of changes in laser power along with changes in the incident laser beam position. By transferring the beam location from A516 steel (-1) to duplex stainless steel (+1), the rate of temperature enhancement was increased significantly with the augmentation of the laser power. At the incident beam power level of 200 W and laser beam irradiation on duplex stainless steel, due to its insufficient melting, the temperature on A516 steel was less than 100 °C around the laser beam irradiation area. With the rise of laser beam power, as a result of creating a molten pool on duplex stainless steel, the temperature of A516 steel was also increased up to about 100 °C. However, when the laser beam was irradiated on A516 steel, the increase in laser power did not change much in the temperature of the area around the melt pool.

Fig. 3 illustrates the effect of incident laser beam power and beam deviation on the temperature of A516 steel. By moving the laser beam location from A516 steel (-1) toward duplex stainless steel (+1), the rate of temperature augmentation was clearly increased with the surge the

Table 4
CCD experimental design matrix.

Exp. No	parameter			
	Power (W)	Speed (mm/min)	Nozzle distance (mm)	Deviation (mm)
1	400	300	55.0	−0.5
2	400	300	50.0	−0.5
3	250	300	55.0	0.5
4	250	200	50.0	−0.5
5	400	200	55.0	−0.5
6	250	200	50.0	0.5
7	250	300	50.0	−0.5
8	400	200	55.0	0.5
9	250	300	50.0	0.5
10	325	250	52.5	−1.0
11	400	300	50.0	0.5
12	325	250	52.5	0.0
13	400	300	55.0	0.5
14	325	250	52.5	1.0
15	250	200	55.0	−0.5
16	325	250	52.5	0.0
17	325	150	52.5	0.0
18	250	200	55.0	0.5
19	475	250	52.5	0.0
20	250	300	55.0	−0.5
21	400	200	50.0	−0.5
22	325	350	52.5	0.0
23	175	250	52.5	0.0
24	400	200	50.0	0.5
25	325	250	52.5	0.0
26	325	250	47.5	0.0
27	325	250	57.5	0.0
28	325	250	52.5	0.0

laser power. At the power of 200 W and laser beam irradiation on duplex stainless steel, due to its insufficient melting, the temperature on A516 steel was less than 100 °C. At higher laser beam power, up to the 500 W, as a result of creating a bigger molten pool on duplex stainless steel, the temperature of A516 steel was also increased up to about 200 °C. Meanwhile, increasing the laser power while irradiation on A516 steel did not create any remarkable changes on the temperature of A516 steel. This is because of the high melting ratio of A516 steel and the low heat transfer rate of duplex steel.

4.2. Effect of welding parameters on the mechanical strength of the joints

The results of the analysis of variance, according to Table 6, the value of Rsq 94 % and the Lack of fit 0.88 showed that the regression model was in a good agreement with the experiment results. Based on the analysis of variance, the incident laser beam power and welding speed, among the linear parameters, had the greatest effect on the weld tensile strength. In regard to the nonlinear square terms, the amount of beam deflection had the most remarkable effect on tensile strength.

The tensile strength regression equation, including linear and nonlinear terms, and the interaction of the parameters is shown by Eq. (2). The square terms of speed, power and speed-power interaction were eliminated in equation (2) because of being insignificant from ANOVA results.

Table 5
Analysis of Variance results for temperature of duplex stainless steel.

Source	DF	Adj SS	Adj MS	F-Value	P-Value
Model	7	52595.4	7513.6	13.64	0.000
Linear	4	33819.2	8454.8	15.34	0.000
Power	1	17550.0	17550.0	31.85	0.000
Speed	1	1962.0	1962.0	3.56	0.074
Noz-dis	1	145.0	145.0	0.26	0.614
Dev	1	14162.0	14162.0	25.70	0.000
2-Way Interaction	3	18776.2	6258.7	11.36	0.000
Power × Dev	1	7788.1	7788.1	14.13	0.001
Speed × Dev	1	4865.1	4865.1	8.83	0.008
Noz-dis × dev	1	6123.1	6123.1	11.11	0.003
Error	20	11020.4	551.0		
Lack-of-Fit	17	8984.4	528.5	0.78	0.688
Pure Error	3	2036.0	678.7		
Total	27	63615.7			
R-sq	R-sq(adj) R-sq(pred)				
82.68 %	76.61 % 63.51 %				

According to Table 6, the three parameters of laser power, square of beam deflection and nozzle distance interaction, and laser beam deflection had the greatest effect on tensile strength.

Fig. 4 shows the incident beam power influence and the amount of the deviation of the laser beam from the contact of two pieces on the tensile strength. It could be observed that the maximum tensile strength was created when the laser beam was in the center of the junction of the two pieces. In this case, the laser beam deflected towards A516 steel, or duplex stainless steel reduced the tensile strength rate. The reason could be the lack of symmetry in the molten pool. Based on the materials' mechanical properties, as depicted in Table 1, failure usually occurs in the tensile test of A516 steel.

Therefore, the lack of complete melting and deflection of the beam towards A516 steel further reduced the mechanical strength, as compared to duplex stainless steel. This is because of the lower strength of the melt pool and the less melting rate of duplex stainless steel, which could reduce the mechanical strength. On the other hand, the deflection of the beam towards the duplex stainless steel, while increasing the mechanical strength, as compared to the beam radiation on A516 steel, reduced the weld strength, relative to the radiation of the beam at the point of the contact between the two parts. The main reason is the separation and failure of the part from A516 steel due to the reduction of the melting volume of A516 steel and the lower strength of this steel, as compared to duplex stainless steel.

On the other hand, as can be observed in Fig. 5, with the rise of the nozzle distance from the surface of the workpiece, the tensile strength was obviously reduced; this reduction rate was higher at the low welding speed of 180 mm/min. At the low speed of 180 mm/min, because of the long interaction time between the laser beam and the material surface, the melting volume was clearly extended, thereby increasing the tensile strength. By increasing the nozzle distance due to the larger diameter of the laser beam and decreasing the laser energy density, the melting volume in duplex stainless steel was reduced; as a result, the tensile strength was decreased too. Also, by moving the beam's focal point to the workpiece subsurface (from 48 to 57 mm), the melting volume of duplex side and tensile strength were reduced.

$$TensileStrength = -237 + 1.3639 \times Power - 0.287 \times Speed + 18.7 \times Noz-dis + 1236 \times Dev - 0.225 \times Noz-dis \times Noz-dis - 108.1 \times Dev \times Dev - 0.158 Power \times Dev - 0.487 \times Speed \times Dev - 19.75 Noz-dis \times Dev \quad (2)$$

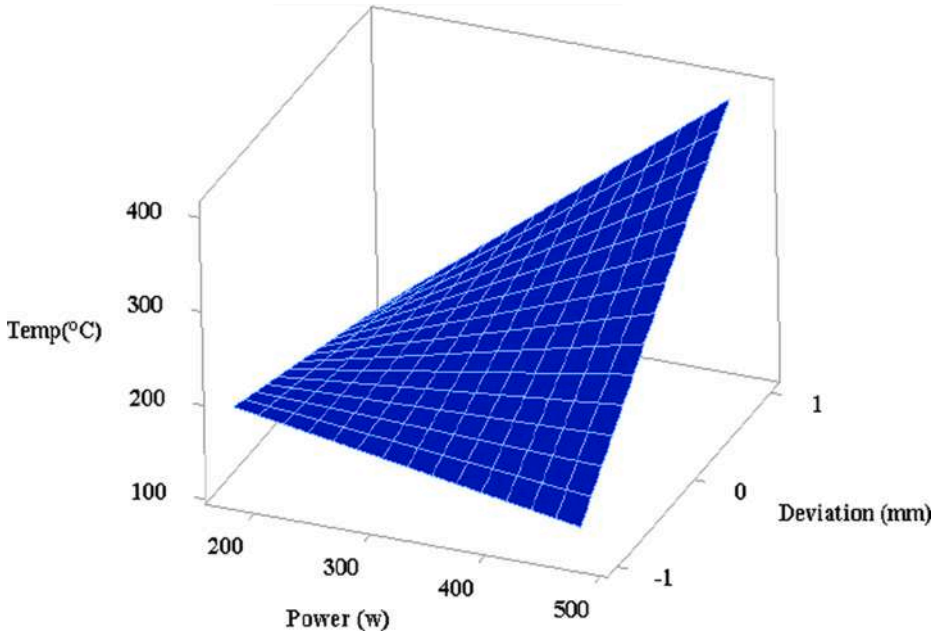

Fig. 2. Influence of the laser power and deviation on the temperature of duplex stainless steel.

4.3. Effect of parameters variation on the depth of the molten pool

The results of the analysis of variance, as shown in Table 7, revealed that the incident laser beam power and the linear speed of welding had a significant effect on the welding depth (with values - Rsq = 91 %, p valve less than 0005 and Lack of fit = 0.697), thus implying that the regression model was well consistent with the experiments. The depth regression equation consisted of linear and nonlinear terms, as depicted by Eq. (3). The square terms of power, speed and speed-power interaction were eliminated in equation (3) because of having more than 3 decimal digits in equation.

$$depth = -2514 + 3.150 \times Power - 1.942 \times Speed + 104 \times Noz-dis + 623 \times Dev - 1.01 \times Noz-dis \times Noz-dis - 105.2 \times Dev \times Dev + 0.250 \times Power \times Dev + 2.325 \times Speed \times Dev - 24.5 \times Noz-dis \times Dev \quad (3)$$

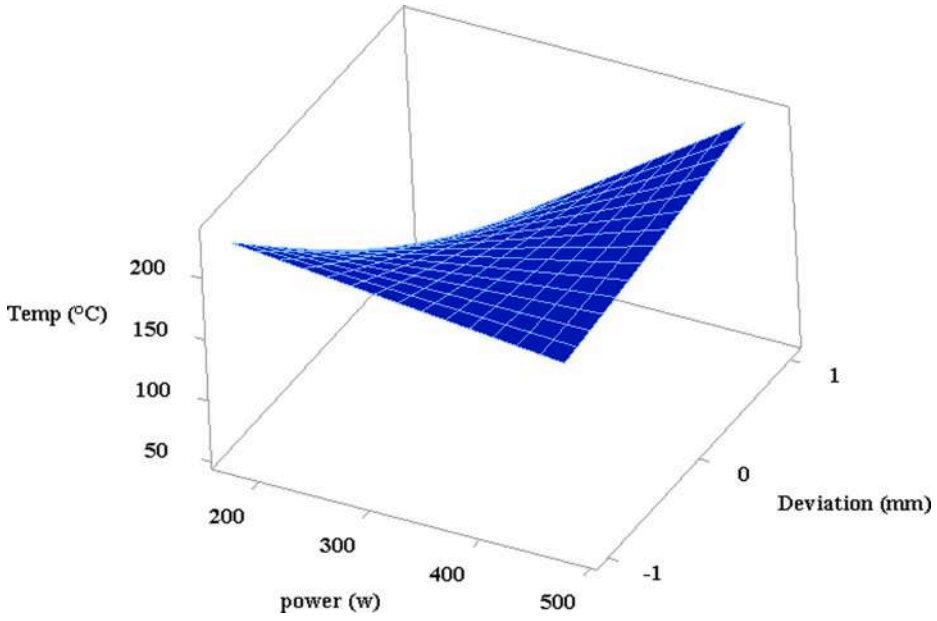

Fig. 3. Influence of the laser power and deviation on the temperature of duplex stainless steel.

Table 6
The results of Analysis of Variance for mechanical strength of the duplex stainless steel and A516 steel.

Source	DF	Adj SS	Adj MS	F-Value	P-Value
Model	9	296,286	32,921	36.05	0.000
Linear	4	263,846	65,961	72.23	0.000
Power	1	251,126	251,126	274.98	0.000
Speed	1	4959	4959	5.43	0.032
Noz-dis	1	3626	3626	3.97	0.062
Dev	1	4134	4134	4.53	0.047
Square	2	19,748	9874	10.81	0.001
Noz-dis × Noz-dis	1	53	53	0.06	0.813
Dev × Dev	1	19,485	19,485	21.34	0.000
2-Way Interaction	3	12,692	4231	4.63	0.014
Power × Dev	1	564	564	0.62	0.442
Speed × Dev	1	2377	2377	2.60	0.124
Noz-dis × Dev	1	9752	9752	10.68	0.004
Error	18	16,439	913		
Lack-of-Fit	15	11,139	743	0.42	0.889
Pure Error	3	5300	1767		
Total	27	312,725			
R-sq 94.74 %	R-sq(adj) 92.12 % R-sq (pred) 88.40 %				

Fig. 6 shows the incident laser beam power and nozzle distance on the melt pool depth. With the increase of the emitted beam power from 200 to 450 W, the penetration depth of laser welding was increased from 300 to 1200 μm. Therefore, changes in laser power due to the increase in laser energy density per unit area had a notable effect on the extension of the weld depth.

The effect of increasing the laser power on the depth of the molten pool could be observed in three irradiated locations on A516 steel, duplex stainless steel and the contact area of the two workpieces, as can be seen in Fig. 6. According to the diagram, the maximum depth of the molten pool and the rate of its increase were on duplex stainless steel. Due to the low heat transfer rate as well as the deflection of the beam towards it, the penetration depth was higher than the beam radiation in the center or the beam radiation on A516 steel.

4.4. Microstructure analysis of dissimilar joint fusion zone

Variations of the microstructure of the weld fusion zone and base metals are depicted in Fig. 7. The A516 steel base metal microstructure was composed of ferrite and pearlite structure, as represented in Fig. 7a. The microstructural changes of the fusion zone and adjacent areas clearly depend on the heating and cooling cycles induced in the weld region. Therefore, the cooling rate shown in the transformation diagram of low carbon steel creates the microstructure composed of acicular ferrite, bainite and martensite [32].

Moreover, the lower heat input rate in HAZ accelerates the cooling of this region and, primarily, the transformation of the microstructure to the martensite. The bulk of fusion zone microstructure was composed of a fully martensitic structure. The temperature of the weld fusion zone reached the upper critical temperature (AC3), which mainly created the austenite microstructure. The severe heat input rate and rapid cooling led to martensite transformation in the fusion zone. The duplex stainless steel microstructure was composed of austenitic grains at the ferrite matrix structure. The HAZ microstructure included δ ferrite grains and austenite phases.

Fig. 8 depicts the microstructure variation from the base metal to the fusion zone of duplex stainless steel. The fusion zone microstructure near duplex stainless steel (DSS) was formed from the distribution difference of ferrite–austenite proportion on different fusion zone areas. The cooling cycle and the amount of heat input could clearly determine the transformation of ferrite grains as austenite grains during the nucleation process. At the fusion line, a lower cooling rate, in comparison to the center of fusion line, led to increasing the formation of austenitic phase, as obtained in other studies [32].

Fig. 9 and Table 8 show different weight percentages of elements from both base metals to the fusion zone of the dissimilar weld. As can be observed in Table 8, the contribution of Cr, Ni and Fe at fusion had the predominant elemental composition in the fusion zone. From the A516 base metal, it could be seen that the Mn and Fe weight percentage was clearly reduced from the A516 steel base metal. At the fusion line from A516 to DSS, the Fe percentage was continually decreased, although Ni and Cr were distributed at the fusion zone with minor changes of weight percentage. It could be, therefore, concluded that Cr and Ni had a crucial effect on elemental alloy's composition in the laser welding process. The Fe element percentage was greatly reduced, about 20 percent, in comparison to the A516 base metal, which was about 13 percent higher than that of the DSS base metal. Although the melting point of A516 steel is about 60 °C more than duplex stainless steel, the phase transformation occurs at the temperature between 850 °C and 900 °C [33]. The phase

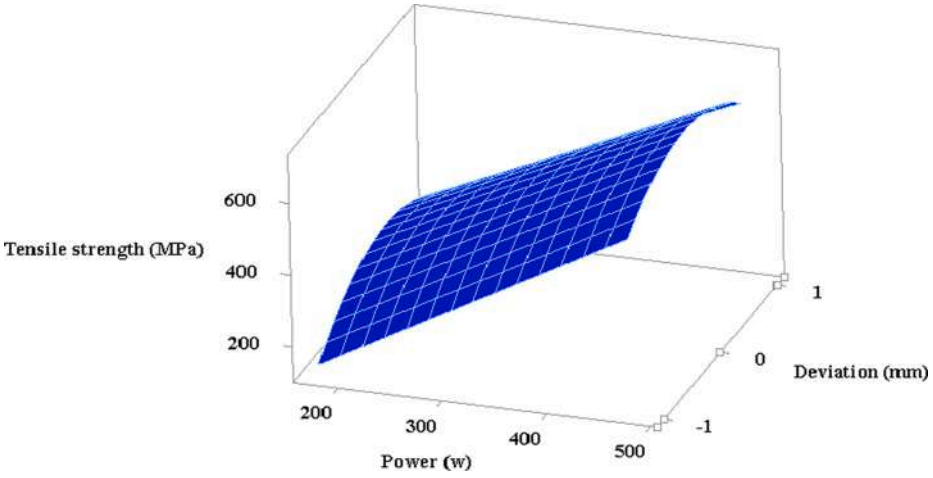

Fig. 4. Effect of incident laser beam power and deviation on the dissimilar joint tensile strength.

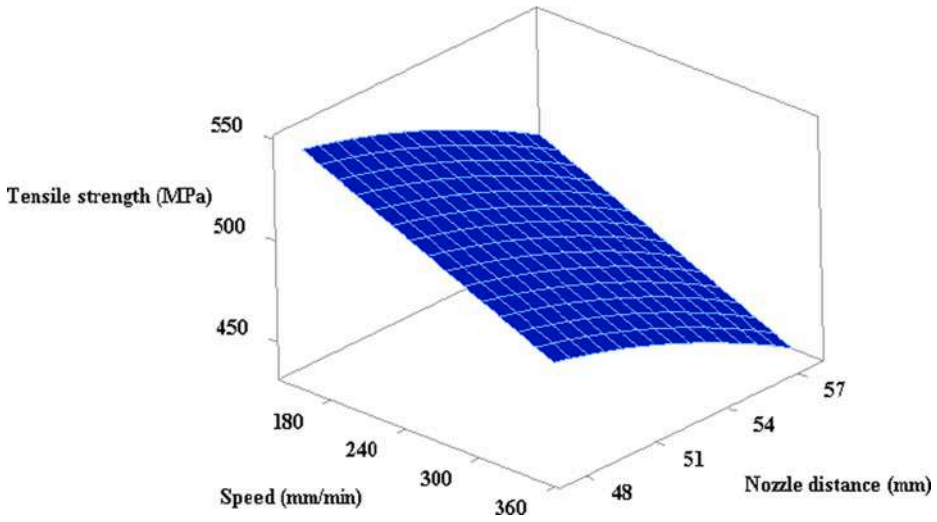

Fig. 5. Effect of linear speed and nozzle distance on the joint tensile strength.

Table 7
Analysis of Variance results for depth of the melt pool.

Source	DF	Adj SS	Adj MS	F-Value	P-Value
Model	9	1,655,717	183,969	20.53	0.000
Linear	4	1,566,683	391,671	43.72	0.000
Power	1	1,339,537	1,339,537	149.51	0.000
Speed	1	226,204	226,204	25.25	0.000
Noz-dis	1	938	938	0.10	0.750
Dev	1	4	4	0.00	0.983
Square	2	18,564	9282	1.04	0.375
Noz-dis × Noz-dis	1	1063	1063	0.12	0.735
Dev × Dev	1	18,463	18,463	2.06	0.168
2-Way Interaction	3	70,469	23,490	2.62	0.082
Power × Dev	1	1406	1406	0.16	0.697
Speed × Dev	1	54,056	54,056	6.03	0.024
Noz-dis × Dev	1	15,006	15,006	1.67	0.212
Error	18	161,269	8959		
Lack-of-Fit	15	127,469	8498	0.75	0.697
Pure Error	3	33,800	11,267		
Total	27	1,816,986			
	R-sq 91.12 % R-sq(adj) 86.69 % R-sq(pred) 76.80 %				

transformation for A516 starts from 700 °C which in turn fully martensitic structure was observed a predominant microstructure of fusion zone in comparison to the as austenite microstructure of duplex stainless steel at an identical welding condition without deviation from the joint attachment line [34].

4.5. Micro-hardness of welded profile

The micro-hardness of dissimilar welded samples, from both base metals to the melt pool, is shown in Fig. 10. The hardness profiles showed that the hardness of the melt pool was evidently lower than that of the A516 steel base metal; meanwhile, the fusion zone hardness of the seams was clearly harder than that of duplex stainless steel base metal. Due to having the combination of both metals in the fusion zone, the maximum hardness values were clearly different from both base metals. The different combination of alloy elements (Ni, Cr, Fe) and microstructures at the fusion zone increased the hardness, in comparison to duplex stainless steel. The average hardness of the fusion zone was about 25 percent higher than that of duplex stainless steel. On the contrary, the hardness of the fusion zone relatively adjacent to A516 steel was remarkably higher because of creating the martensitic microstructure,

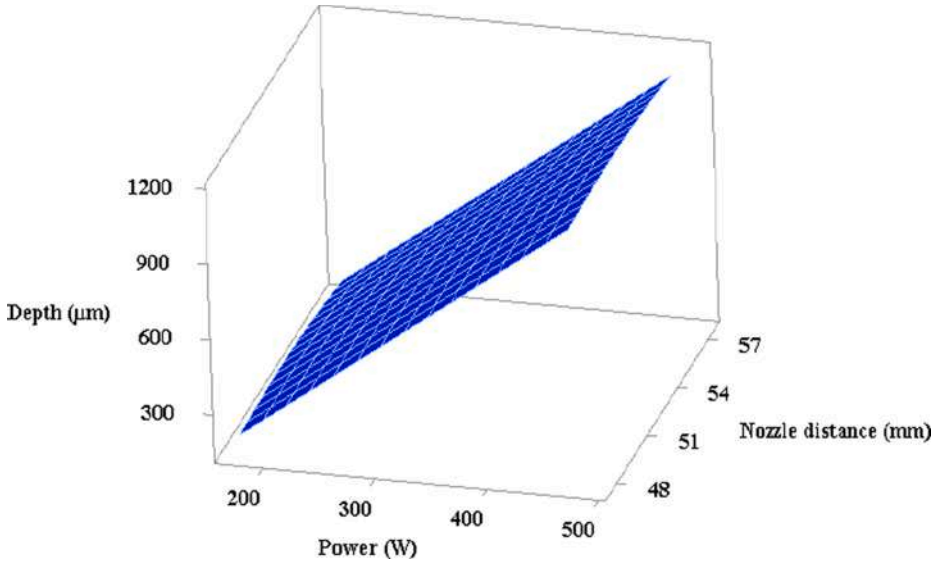

Fig. 6. Effect of incident beam power and nozzle distance on depth of the melt pool.

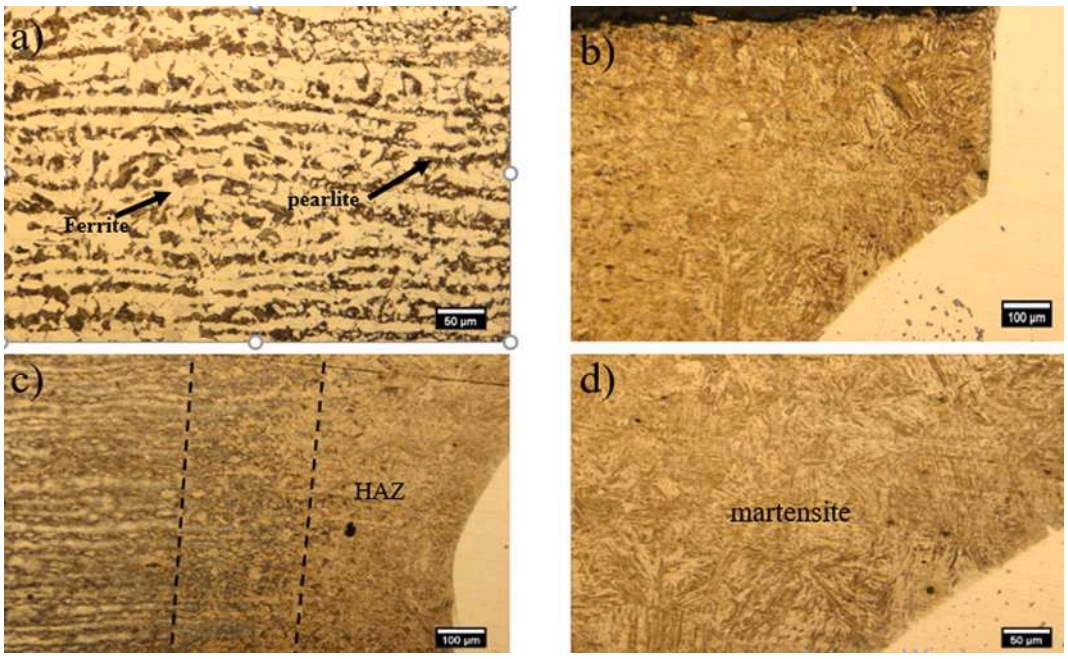

Fig. 7. Microstructure of A516 steel at different areas for a) base metal, b) fusion line, c) HAZ, d) fusion zone.

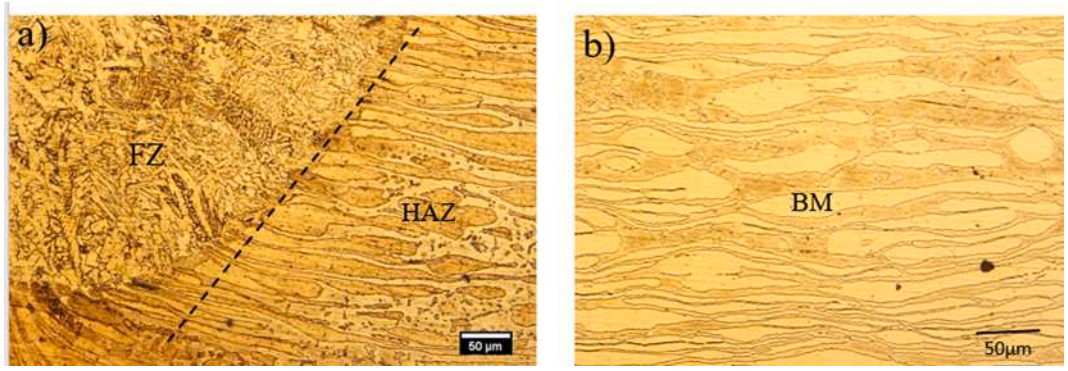

Fig. 8. Microstructure of duplex stainless steel for a) weld fusion zone and HAZ, b) for base metal.

according to the high temperature gradient of the laser beam. Furthermore, increasing laser power induced higher temperature gradient; this, in turn, created a higher percentage of martensite structure at the A516 steel side and enhanced the ferrite concentration at the duplex stainless steel side of the fusion zone. Hence, increasing both martensite volume and ferrite concentration clearly caused higher hardness, as also reported by Soltani and Tayebi [35].

4.6. Tensile properties of the welded samples

The dissimilar welded joints' mechanical properties were evaluated in terms of tensile strength and elongation percentage with three repetitions for each test condition. The effects of laser beam power and nozzle distance on both ultimate tensile strength and percentage of elongation were evaluated. Tensile tests were conducted at the welding speed of 2 mm/ min. The maximum tensile strength of welded samples belonged to the laser power of 400 W and welding speed of 300 mm/min at the focal point (the nozzle distance of 5 mm from the workpiece surface). The maximum tensile strength of 500 MPa and 18 percent elongation were obtained under this condition. The sample was fractured from A516 carbon steel due to having lower mechanical properties, in comparison to DSS (see Fig. 11). Increasing the focal point distance evidently reduced the laser beam power density and hence, the weld penetration into the materials thickness. Hence, the tensile strength of these samples of the 6 mm adjusted point from the focal point was remarkably decreased, about 30 percent; also, on average, there was about 50 % reduction of elongation. As depicted in Fig. 11, the welded samples were fractured from the weld region. All dissimilar laser welded samples had lower tensile strength and elongation percentage in comparison to the A516 base metal. It could be inferred that coarse grains and martensite transformed into the austenite structure led to the lower tensile strength and elongation. Because of having lower energy density in the fusion zone of the samples No 3 and 15, loss of ductility was observed, as shown in Fig. 12c. Evidently, the fracture happened at the fusion zone. Other samples showed more ductility, which was similar to the A516 fracture surface with bigger and deeper fracture dimples, as

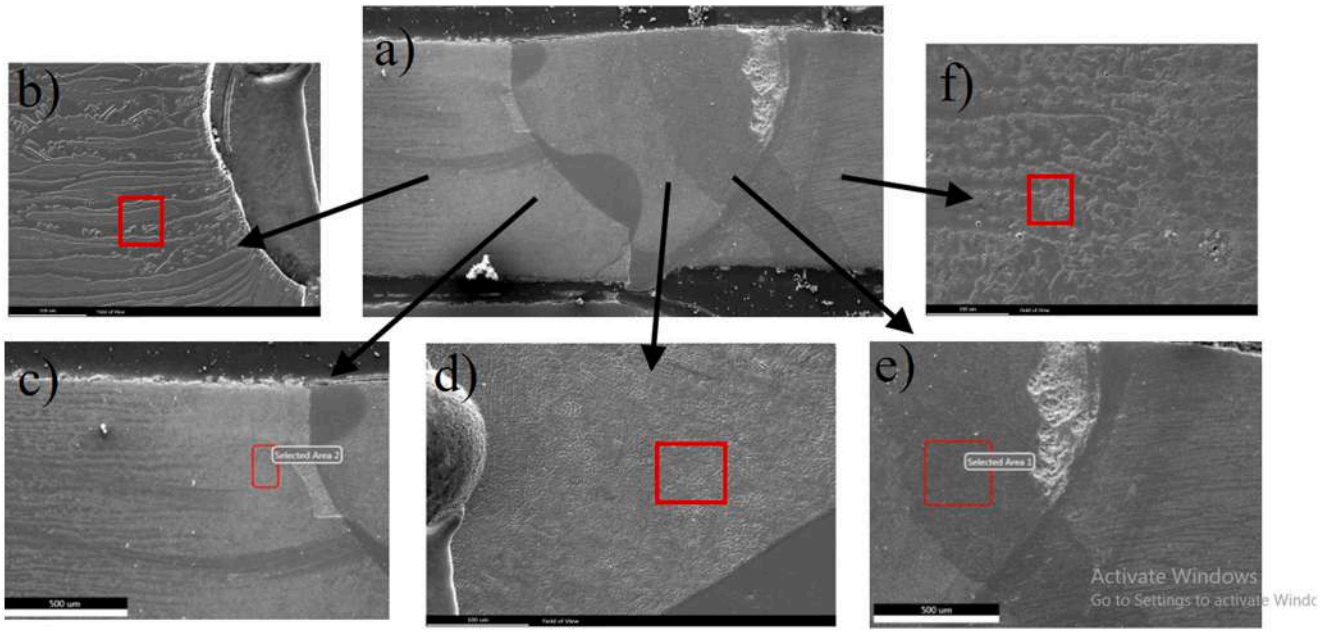

Fig. 9. Location of different points for EDS analysis from A516 at regions of base metal to the fusion zone of b) A516 base metal,c) A516 HAZ, d) fusion zone at A516 side, e) duplex side fusion zone, f) Duplex HAZ.

Table 8
EDS analysis results based on weight percentage.

Area	Elements	Weight %
b	Si	0.13
	Mn	1.06
	Fe	98.87
c	Si	0.13
	Mn	0.96
	Fe	98.91
d	Si	0.12
	Cr	16.1
	Ni	4.84
	Fe	78.9
e	Si	0.01
	Cr	15.79
	Ni	4.65
	Fe	79.56
f	Si	0.27
	Cr	25.4
	Ni	7.9
	Fe	66.46

can be seen in Fig. 12 a, b. Apparently, higher laser energy density effectively improved the fracture ductility of the welded samples.

5. Conclusion

- Dissimilar laser welding of A516 steel to duplex stainless steel was performed to evaluate the effect of parameters on the temperature field, tensile strength, depth of melt pool and microstructure of the weld joint. The incident laser beam power and laser beam deflection had the most remarkable effect on the measured melt pool temperature adjacent areas. Also, the interaction of laser power and beam deflection had more effect on the temperature around the molten pool of duplex stainless steel.
- The maximum tensile strength of 500 MPa and 18 percent elongation were obtained at the laser power of 400 W and welding speed of 300 mm/min at the focal point (nozzle distance of 5 mm from the workpiece surface.)
- Emitted laser beam power and linear speed of welding, among the linear parameters, had a more significant effect on the tensile strength of the weld. Among the nonlinear square terms, the amount of beam deflection had the most remarkable effect on tensile strength.
- The weld fusion zone microstructure of A516 side was composed of a fully martensitic structure.
- The higher heat input upper critical temperature (AC3) and rapid cooling led to martensite transformation, mainly in the fusion zone of the weld metal.
- The microstructure of duplex stainless steel was composed of austenitic grains on the ferrite matrix structure. The HAZ microstructure included δ ferrite grains and austenite phases.
- Increasing the laser power created a higher temperature gradient which led to the higher percentage of martensite structure at the A516 steel side and enhanced the ferrite concentration at the duplex stainless steel side of the fusion zone. Hence, the hardness of the fusion zone was about 25 percent higher than that of duplex stainless steel. On the contrary, the hardness of the fusion zone adjacent to A516 steel was remarkably higher because of creating the martensitic microstructure.
- The ductility of the A516 fracture surface with bigger and deeper fracture dimples was caused by applying higher laser energy density, which effectively improved the fracture ductility of the welded samples.

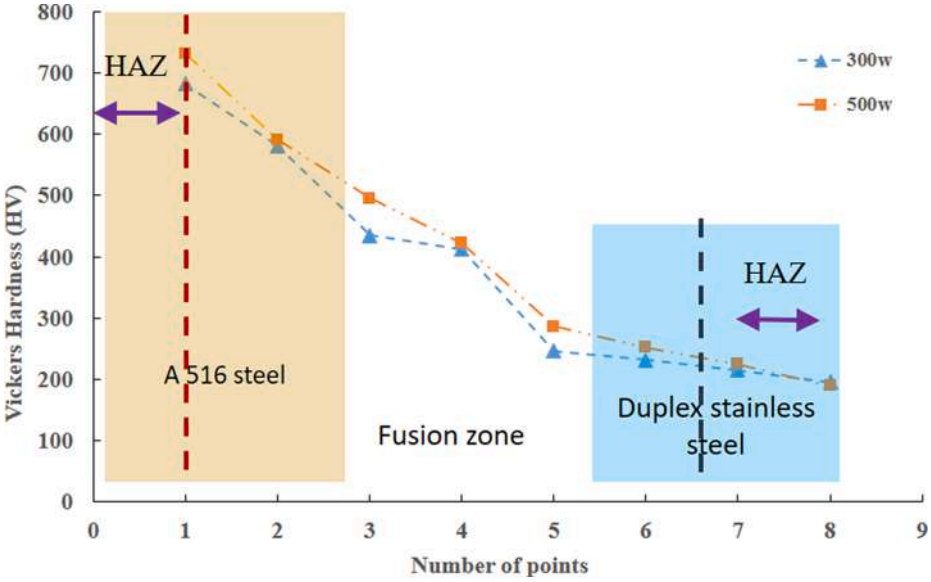

Fig. 10. Microhardness of welded samples at weld region.

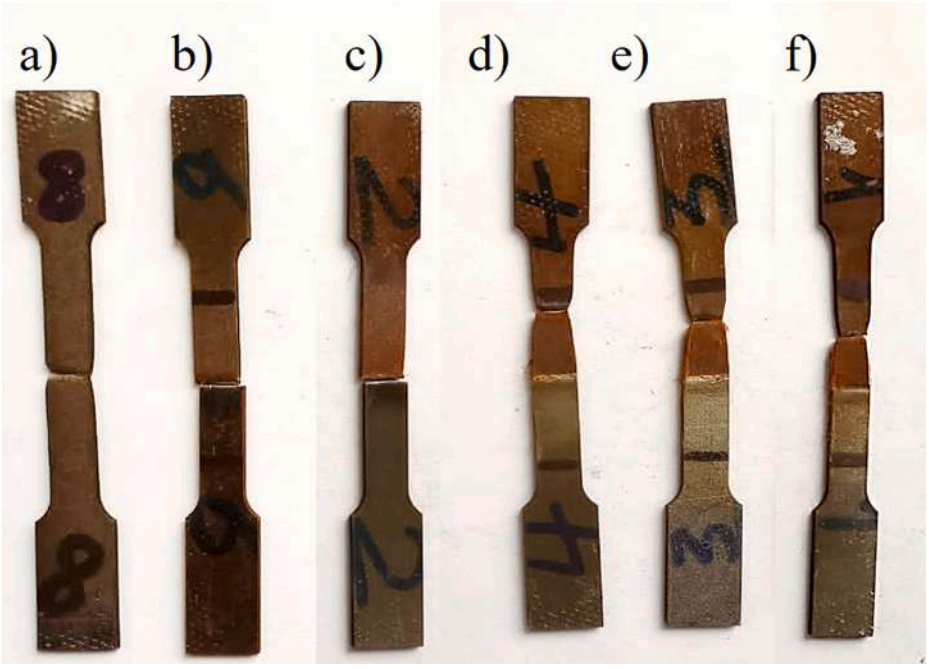

Fig. 11. Failure appearance of tensile tests of welded samples for EXP No. of a) 3, b) 15, c) 27, d) 19, e) 17, f) 24.

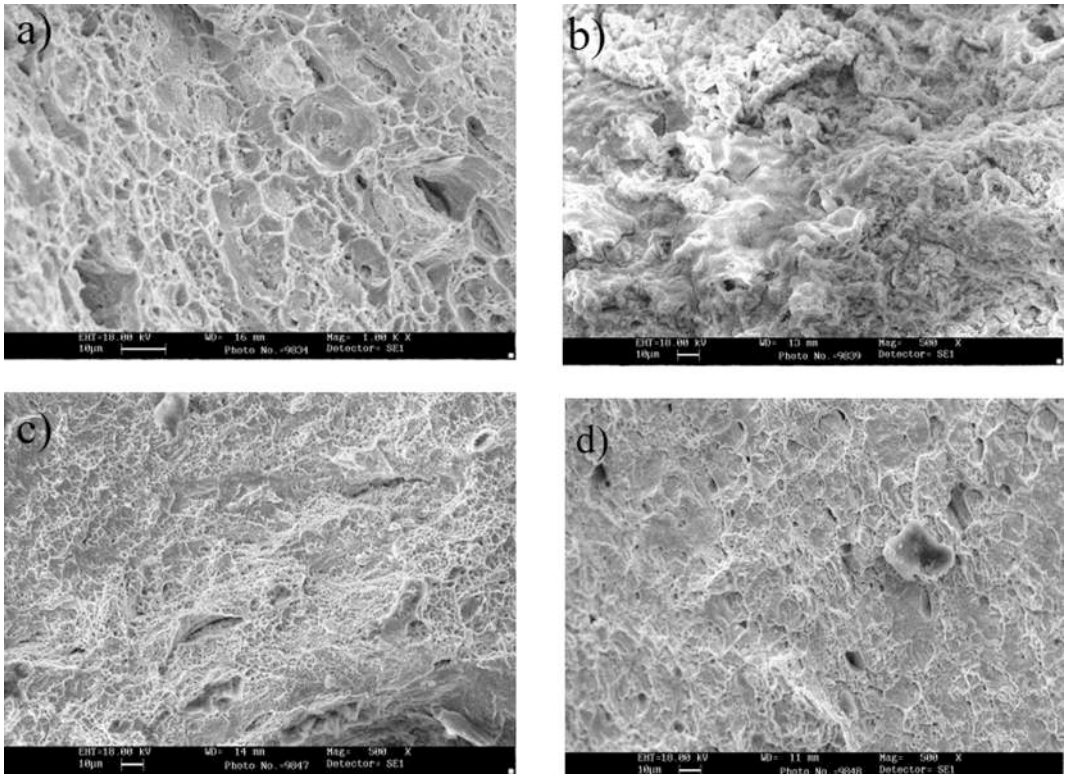

Fig. 12. Appearance of the fracture surface of the tensile tests samples for Exp. No of a) 27, b) 19, c)15, d)27.

Declaration of Competing Interest

The authors declare that they have no known competing financial interests or personal relationships that could have appeared to influence the work reported in this paper.

Data availability

The authors do not have permission to share data.

References

[1] K. Devendranath Ramkumar, D. Mishra, M.K. Vignesh, B. Ganesh Raj, N. Arivazhagan, S.V. Naren, S. Suresh Kumar, Metallurgical and mechanical characterization of electron beam welded super-duplex stainless steel UNS 32750, J. Manuf. Process. 16 (4) (2014) 527–534.

[2] S. Saravanan, K. Raghukandan, N. Sivagurumanikandan, Pulsed Nd: YAG laser welding and subsequent post-weld heat treatment on super duplex stainless steel, J. Manuf. Process. 25 (2017) 284–289.

[3] Y.S. Sato, T.W. Nelson, C.J. Sterling, R.J. Steel, C.-O. Pettersson, Microstructure and mechanical properties of friction stir welded SAF 2507 super duplex stainless steel, Mater. Sci. Eng. A 397 (1-2) (2005) 376–384.

[4] P. Luchtenberg, P.T. de Campos, P. Soares, C.A.H. Laurindo, O. Maranho, R. D. Torres, Effect of welding energy on the corrosion and tribological properties of duplex stainless steel weld overlay deposited by GMAW/CMT process, Surf. Coat. Technol. 375 (2019) 688–693.

[5] S. Saravanan, N. Sivagurumanikandan, K. Raghukandan, Effect of process parameters in microstructural and mechanical properties of Nd: YAG laser welded super duplex stainless steel, Mater. Today:. Proc. 39 (2021) 1248–1253.

[6] N.K. Adomako, G. Shin, N. Park, K. Park, J.H. Kim, Laser dissimilar welding of CoCrFeMnNi-high entropy alloy and duplex stainless steel, J. Mater. Sci. Technol. 85 (2021) 95–105.

[7] G.N. Ahmad, M.S. Raza, N.K. Singh, H. Kumar, Experimental investigation on Ytterbium fiber laser butt welding of Inconel 625 and Duplex stainless steel 2205 thin sheets, Opt. Laser Technol. 126 (2020), 106117.

[8] A. Baghdadchi, V.A. Hosseini, K. Hurtig, L. Karlsson, Promoting austenite formation in laser welding of duplex stainless steel—impact of shielding gas and laser reheating, Welding in the World 65 (3) (2021) 499–511.

[9] I. Calliari, C. Gennari, E. Hurtado Delgado, A.F. Miranda Perez, B.R. Rodriguez Vargas, Laser welding of plastically deformed lean duplex stainless steel, Metallurgia Italiana 1 (2018) 5–10.

[10] L. Chen, C. Wang, X. Zhang, G. Mi, Effect of parameters on microstructure and mechanical property of dissimilar joints between 316L stainless steel and GH909 alloy by laser welding, J. Manuf. Processes 65 (2021) 60–69.

[11] Ghosh, Aritra, Paramasivan Kalvettukaran, Dipten Misra, and Sanjib Kumar Acharyya. "Experimental Investigation on the Effect of Pulse Width on Laser Welding of 2205 Duplex Stainless Steel.".

[12] H. Gozarganji, A. Farnia, M. Ebrahimnia, Effect of shielding gas composition on geometry and austenite formation in low power pulsed Nd: YAG laser welded 2205 duplex stainless steel, Arch. Metall. Mater. 66 (2021).

[13] M. Landowski, Influence of parameters of laser beam welding on structure of 2205 duplex stainless steel, Advances in Materials Science 19 (2019) 21–31.

[14] N. Sivagurumanikandan, S. Saravanan, G. Shanthos Kumar, S. Raju, K. Raghukandan, Prediction and optimization of process parameters to enhance the tensile strength of Nd: YAG laser welded super duplex stainless steel, Optik 157 (2018) 833–840.

[15] R. Oyyaravelu, P. Kuppan, N. Arivazhagan, Metallurgical and mechanical properties of laser welded high strength low alloy steel, J. Adv. Res. 7 (3) (2016) 463–472.

[16] M. Salavati, Y. Mazaheri, M. Sheikhi, Effect of ND: YAG Pulsed Laser Welding Parameters on Microstructural Evolutions and Mechanical Properties of 2205 Duplex Stainless Steel, Modares Mechanical Engineering 19 (10) (2019) 2535–2541.

[17] M. Mozafarifard, D. Toghraie, Time-fractional subdiffusion model for thin metal films under femtosecond laser pulses based on Caputo fractional derivative to examine anomalous diffusion process, Int. J. Heat Mass Transf. 153 (2020), 119592.

[18] M. Mozafarifard, S.M. Mortazavinejad, D. Toghraie, Numerical simulation of fractional non-Fourier heat transfer in thin metal films under short-pulse laser, Int. Commun. Heat Mass Transfer 115 (2020), 104607.

[19] R. Abedinzadeh, E. Norouzi, D. Toghraie, Experimental investigation of machinability in laser-assisted machining of aluminum-based nanocomposites, J. Mater. Res. Technol. 15 (2021) 3481–3491.

[20] X.U. Shumin, L.I. Weijie, L.I.U. Xianglei, et al., Performance Analysis of Plastic Deformation Inertial Control Switch Based on 3D Printing[J], Journal of Ordnance Equipment Engineering 42 (05) (2021) 244–249.

[21] D.I. Chengkuan, H.U.A.N.G. Shutao, Y.U. Xiaolin, et al., Effect of Cutting Tool Materials on Temperature Field of Cutting AF1410 High Strength Steel[J]. *Journal of Ordnance Equipment*, Engineering 42 (06) (2021) 243–250.

[22] L.I.U. Zhengtao, L.I. Zhongsheng, C.H.E.N. Dajun, et al., Research Status of Friction Stir Welding of Ti/Al Dissimilar Metals[J], Journal of Ordnance Equipment Engineering 42 (08) (2021) 106–111.

[23] B.J. Lv, S. Wang, T.W. Xu, F. Guo, Effects of minor Nd and Er additions on the precipitation evolution and dynamic recrystallization behavior of Mg–6.0 Zn–0.5 Mn alloy, J. Magnesium Alloys 9 (3) (2021) 840–852.

[24] B. Zhang, Z. Wang, H. Yu, Y. Ning, Microstructural origin and control mechanism of the mixed grain structure in Ni-based superalloys, J. Alloy. Compd. 900 (2022), 163515.
[25] X. Li, X. Yang, D. Yi, B. Liu, J. Zhu, J. Li, C. Gao, L. Wang, Effects of NbC content on microstructural evolution and mechanical properties of laser cladded Fe50Mn30Co10Cr10-xNbC composite coatings, Intermetallics 138 (2021), 107309.
[26] T. Xin, S. Tang, F. Ji, L. Cui, B. He, X. Lin, X. Tian, H. Hou, Y. Zhao, M. Ferry, Phase transformations in an ultralight BCC Mg alloy during anisothermal ageing, Acta Mater. 239 (2022), 118248.
[27] L. Liang, M. Xu, Y. Chen, T. Zhang, W. Tong, H. Liu, H. Wang, H. Li, Effect of welding thermal treatment on the microstructure and mechanical properties of nickel-based superalloy fabricated by selective laser melting, *Materials Science and Engineering*: *A* 819 (2021), 141507.
[28] Y. Wu, J. Chen, L. Zhang, J. Ji, Q. Wang, S. Zhang, Effect of boron on the structural stability, mechanical properties, and electronic structures of γ′-Ni3Al in TLP joints of nickel-based single-crystal alloys, Mater. Today Commun. 31 (2022), 103375.
[29] Y. Yang, Y. Gong, C. Li, X. Wen, J. Sun, Mechanical performance of 316 L stainless steel by hybrid directed energy deposition and thermal milling process, J. Mater. Process. Technol. 291 (2021), 117023.
[30] ASM Handbook 13B (2005).
[31] Materials Handbook A Concise Desktop Reference, springer, 2018.
[32] N. Sivagurumanikandan, S. Saravanan, G. Sivakumar, K. Raghukandan, Process window for Nd: YAG laser welding of super duplex stainless steel, J. Russ. Laser. Res. 39 (2018) 575–584.
[33] G. Straffelini, S. Baldo, I. Calliari, E. Ramous, Effect of Aging on the Fracture Behavior of Lean Duplex Stainless Steels, Metall. Mater. Trans. A 40 (2009) 2616–2621.
[34] ASM Handbook, VOL3, Alloy Phase Diagrams,1992.
[35] H.M. Soltani, M. Tayebi, Comparative study of AISI 304L to AISI 316L stainless steels joints by TIG and Nd: YAG laser welding, J. Alloy. Compd. 767 (2018).